IEEE Access
Multidisciplinary | Rapid Review | Open Access Journal

Received March 25, 2021, accepted March 27, 2021, date of publication April 1, 2021, date of current version April 12, 2021.

Digital Object Identifier 10.1109/ACCESS.2021.3070366

Integrated Motion Control Using a Semi-Active Damper System to Improve Yaw-Roll-Pitch Motion of a Vehicle

WANKI CHO[1], JONGSANG SUH[2], AND SEUNG-HAN YOU[1]
[1]School of Mechanical Engineering, Korea University of Technology & Education, Cheonan 31253, South Korea
[2]Phantom AI, Burlingame, CA 94010, USA

Corresponding author: Seung-Han You (shyoo@koreatech.ac.kr)

This work was supported in part by the Hyundai Motor Group, and in part by the National Research Foundation of Korea (NRF) Grant funded by the Korean Government (MSIT) under Grant NRF-2017R1A1A1A05069503.

ABSTRACT This paper describes a new suspension control logic to improve the yaw-roll-pitch motion of vehicles equipped with electronic controlled suspension (ECS). The proposed suspension control logic can simultaneously control the yaw rate, roll, and pitch behavior of a vehicle while also offering the ability to tune the weightings of each degree of freedom (i.e. the yaw rate, roll and pitch control). This algorithm consists of an integrated vehicle observer (IVO) that estimates the vehicle state, an integrated target generator (ITG), an integrated vehicle controller (IVC) and an optimal distribution controller (ODC). The ITG determines the target roll angle, pitch angle, and yaw rate. To achieve these targets, the IVC determines target roll, pitch, and yaw moments. In consideration of the performance limitations of the ECS system, as well as how the system has been tuned, the ODC determines the damping forces to be applied at each wheel through an optimization method. Simulated and experimental tests were conducted to investigate the performance of the proposed control system, the results indicate that the proposed algorithm noticeably improves the yaw-roll-pitch motions of vehicles.

INDEX TERMS Integrated motion control, electronic controlled suspension (ECS), integrated target generator (ITG), integrated vehicle controller (IVC), optimal distribution controller (ODC).

I. INTRODUCTION

Electronic controlled suspension (ECS) is a semi-active damper system that is generally applied to mass-produced luxury vehicles, various types of ECS have developed [1], [2]. The ride comfort and handling performance of vehicles with ECS can be improved by adjusting the damper characteristics according to the driving situation. ECS has the advantage of giving a lot of freedom in terms of motion control because the damper characteristics for each wheel can be controlled independently. However, the performance of this system is somewhat limited because ECS is not an active system but is semi-active [3], [4]. Therefore, many studies have introduced active suspension control methods more widely than semi-active suspension control methods [5]–[7]. Additionally, most studies on semi-active suspension control have focused on controlling a single degree of freedom due to the limited performance of such systems [8]–[12]. Practical multi-objective control methods and extreme machine learning methods have been proposed to improve ride comfort in vehicles with ECS [9], [10]. In addition to these studies, methods for robust H infinity control and for robust sliding mode control have also been investigated to improve ride comfort [11], [12]. A roll control algorithm for sport utility vehicles based on the steering-input-augmented skyhook control strategy has also been introduced [13]. In order to improve the lateral stability of vehicles, a study into a method for integrating braking and semi-active suspension systems has been proposed [14]. In the case of this algorithm, the semi-active suspension control algorithm was designed based on the concept of assisting the lateral stability control by braking. The semi-active suspension system in that algorithm was used to control the yaw rate of the vehicle. In another study, an integrated chassis control method for use with active front steering, a direct yaw moment system, and active suspension was developed to improve both the lateral

The associate editor coordinating the review of this manuscript and approving it for publication was Bidyadhar Subudhi.

and vertical dynamics of the vehicle [15]. That algorithm used active front steering and direct yaw moment systems to improve the lateral dynamics and used the active suspension to improve the vertical dynamics. In this way, many studies that look to control one aspect of vehicle behavior such as roll angle or yaw rate using ECS systems have been conducted but no studies have been conducted that look to control all these behaviors at the same time. The yaw rate, roll angle, and pitch angle of a vehicle are important factors for both ride comfort and handling performance, as such, these behaviors need to be independently controlled in a balanced manner to achieve desirable overall vehicle dynamics. In this paper, we present an integrated motion control algorithm that can control the yaw rate, roll, and pitch behavior of vehicles simultaneously using ECS. In addition, the algorithm is designed to maximize tracking performance of these behaviors or to ensure harmonic performance between behaviors as needed. The proposed algorithm consists of four modules: (i) an integrated vehicle observer (IVO), (ii) an integrated target generator (ITG), (iii) an integrated vehicle controller (IVC), and (iv) an optimal distribution controller (ODC). The IVO estimates vehicle speed, tire load, roll angle, lateral slip angle, and damper speed of each wheel, all of which cannot be measured directly. The ITG computes the target roll angle, the target pitch angle, and the target yaw rate for a given steering angle and vehicle speed. The IVC determines the roll, pitch and yaw moments to track the target behavior for roll angle, pitch angle, and yaw rate. The ODC then computes the ECS damping forces to apply at each wheel to track the control moments obtained by the IVC. Especially, the ODC should track the control moments from the IVC, consider the performance limits of the ECS system, and ensure that control parameter tuning can be carried out in various test scenarios. An optimization approach is applied to the ODC logic to satisfy all these requirements. In order to evaluate the performance of the proposed integrated control algorithm, simulated and experimental tests were conducted on an asphalt road. The vehicle states required for the proposed control algorithm, i.e. such as vehicle speed, damper speed, tire load, etc., are assumed to be know because there are many previous studies on estimation methods for these quantities [16]–[20]. Jin *et al.* proposed a dual unscented Kalman filter approach to estimate vehicle states such as longitudinal velocity and side slip angle and vehicle parameters such as inertial parameters [16]. Cho *et al.* and Rezaeian *et al.* introduced methods that used a random-walk Kalman filter and an unscented Kalman filter, respectively, to estimate longitudinal/lateral/vertical tire forces [17], [18]. An extended state observer (ESO) was developed by Pan *et al.* to estimate a suspension velocity [19]. Li *et al.* proposed a new side-slip angle estimation method based on a lateral dynamics model [20]. Since the signals required for the proposed control algorithm can be sufficiently estimated using methods outlined in various previous studies, the estimation module, the IVO, will not be introduced in this paper.

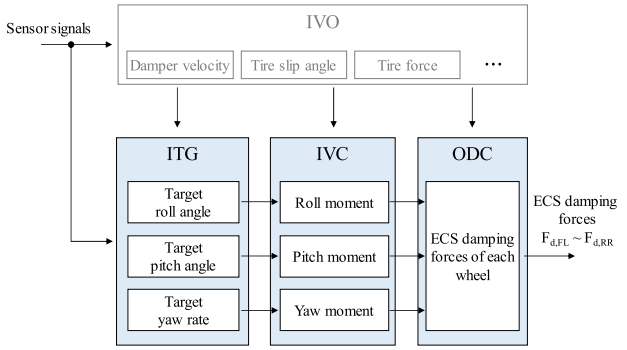

FIGURE 1. Structure of the proposed control system.

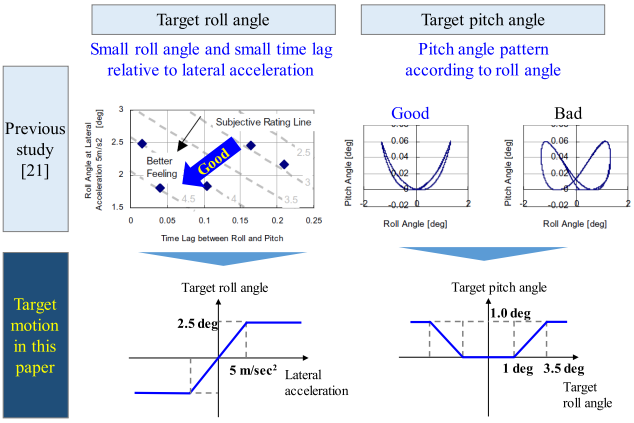

FIGURE 2. Target roll and pitch motions.

This paper is structured as follows: Section II describes the proposed control algorithm. Evaluation results are discussed in section III. Section IV summarizes the contribution of this research and introduces future work.

II. CONTROL ALGORITHM

Fig. 1 shows the overall architecture of the proposed algorithm which consists of four parts: IVO, ITG, IVC, and ODC. The IVO estimates several of the vehicle states necessary for the proposed algorithm. The ITG calculates the target roll angle, pitch angle, and yaw rate. The IVC computes the roll, pitch, and yaw moments. The ODC distributes the ECS damping forces to each wheel.

A. INTEGRATED TARGET GENERATOR (ITG)

In the ITG, the target roll angle, pitch angle, and yaw rate of the vehicle are determined based on work introduced in previous studies.

1) TARGET ROLL ANGLE AND TARGET PITCH ANGLE

In previous studies, two criteria have been defined to determine the target roll and pitch angles [21].

- Criteria 1 (Target roll angle).
  A fast roll response and small roll angle should occur for a lateral acceleration.
- Criteria 2 (Target pitch angle)

According to the roll angle, the pitch angle should be generated according to a given pattern (refer to Fig. 2).

The target roll angle and the target pitch angle are defined based on these two criteria, as shown in Fig. 2. In more detail, the target roll angle is found using a predefined map from the lateral acceleration, the target pitch angle is determined using a predefined map from the target roll angle.

2) TARGET YAW RATE

In order to define the target yaw rate, a bicycle model is used. The target yaw rate is computed as a steady state yaw rate from the bicycle model in [22].

$$\gamma_d = \frac{1}{1 - \frac{m(l_f \cdot C_f - l_r \cdot C_r)v_x^2}{2 \cdot C_f \cdot C_r (l_f + l_r)^2}} \frac{v_x}{l_f + l_r} \delta_f \tag{1}$$

where, δ_f denotes the human driver steering angle; l_f and l_r denote the distance from the center of gravity to front and rear axle, respectively; m denotes the mass of the vehicle; C_f and C_r denote the lateral cornering stiffness of the front and rear tires, respectively; V_x denotes the longitudinal speed.

In general, the target yaw rate is determined by applying a time delay to the steady state yaw rate to match a phase of the actual yaw rate. However, in order to obtain a fast and direct yaw response from the driver's steering input, the target yaw rate is defined as a steady state yaw rate.

B. INTEGRATED VEHICLE CONTROLLER (IVC)

To track the target behaviors (roll angle, pitch angle, and yaw rate) from the ITG, the IVC computes the target roll moment ($M_{x,tar}$), the target pitch moment ($M_{y,tar}$), and the target yaw moment ($M_{z,tar}$). Target control inputs are calculated using PD control.

$$\begin{aligned} M_{x,tar} &= K_{p,roll} \cdot (\phi_{tar} - \phi) + K_{d,roll} \cdot \left(\dot{\phi}_{tar} - \dot{\phi}\right) \\ M_{y,tar} &= K_{p,pitch} \cdot (\theta_{tar} - \theta) + K_{d,pitch} \cdot \left(\dot{\theta}_{tar} - \dot{\theta}\right) \\ M_{x,tar} &= K_{p,yaw} \cdot (\gamma_{tar} - \gamma) + K_{d,yaw} \cdot (\dot{\gamma}_{tar} - \dot{\gamma}) \end{aligned} \tag{2}$$

where, M_x, M_y, and M_z denote the roll, pitch and yaw moments, respectively; subscripts p and d below K denote the proportional and derivative gain, respectively; subscripts roll, pitch, and yaw below K denote the roll, pitch and yaw gain, respectively; subscript tar denotes the target motion of each angle; ϕ, θ, and γ denote roll, pitch and yaw angles, respectively.

C. OPTIMAL DISTRIBUTION CONTROLLER (ODC)

The ODC is the core module in the proposed control algorithm. The ODC computes the damping forces needed to generate the roll, pitch and yaw moments while considering the limitations of the ECS actuators. Fig. 3 shows a block diagram of the ODC. This module consists of the 1st unconstrained optimization module, the control value compensation module, and the 2nd unconstrained optimization module.

The 1st unconstrained optimization module computes the optimal ECS damping force at each wheel without considering any actuator limitations. The control value compensation

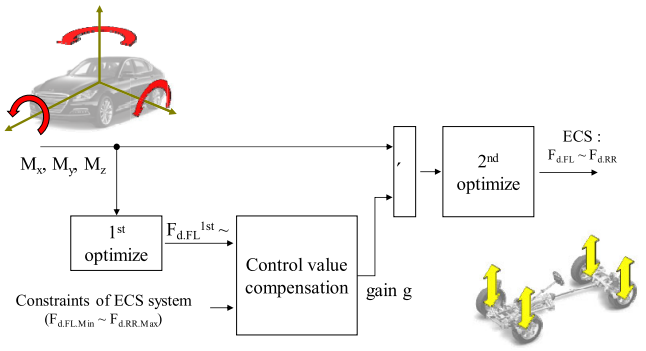

FIGURE 3. Structure of optimal distribution controller.

module derives the "gain g" values to consider the actuator limitations. Using the "gain g" and the target moments, the 2nd optimization module determines the final damping force to be applied by the ECS. The 1st and 2nd optimization modules are identical. The proposed ODC algorithm has the following advantages:

- Low computational load
  The ECS system has min/max performance limitations. An optimization problem with these constraints would require an iterative computation not suitable for real-time computation. However, the proposed ODC algorithm does not use iterative computation.
- Easy weight assignment between roll/pitch/yaw motions
  Since an optimization method is applied, the weight tuning between the target moments is easy. The relative importance of roll angle, pitch angle and yaw rate can be adjusted as needed during vehicle testing.
- Control performance balancing: Tracking/Harmonic
  In this paper, the performance of the proposed controller is determined in two categories: tracking and harmonic performance. Tracking performance measures how overall tracking performs for the target roll moment, pitch moment and yaw moment. Harmonic performance measures how the roll, pitch, and yaw moments are tracked in balance with each other, even if the overall tracking performance is not good. Fig. 4 shows a conceptual diagram of how tracking performance and harmonic performance are related. Since the performance limitations of the ECS are obvious, the damping forces computed in the 1st optimization module exceed the limits of the system in most cases. Most of these damping forces used the ECS system to its limit, so the overall tracking performance for the target roll moment, the target pitch moment, and the target yaw moment can be maximized. However, this approach cannot guarantee balanced tracking performance between each degree of freedom. The balance of control between each degree of freedom (the harmonic performance) is an important factor when evaluating the ride comfort and handling of a vehicle. The ODC can adjust the performance between tracking and

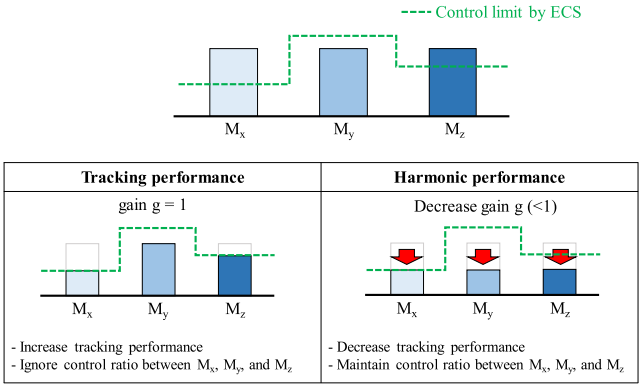

FIGURE 4. Performance tuning for adjusting gain g.

harmonic using the ''gain g''. The ''gain g'' is used to adjust the IVC control inputs as the value to consider the performance limitations of the ECS system. How the performance between tracking and harmonic is adjusted using ''gain g'' can be seen in Fig. 4.

1) UNCONSTRAINED OPTIMIZATION MODULE

In order to apply the optimization approach, it is necessary to derive the relationship between input and output signals. The inputs are the roll, pitch, and yaw moments from the IVC, the outputs are the ECS damping force at each wheel. Since the roll and pitch moments are directly related to the vertical behavior of the vehicle, the equations for roll and pitch motion can be determined as follows:

$$\begin{aligned} M_x &= \frac{t_f}{2}\left(F_{b,FL} - F_{b,FR}\right) + \frac{t_r}{2}\left(F_{b,RL} - F_{b,RR}\right) \\ M_y &= -l_f\left(F_{b,FL} + F_{b,FR}\right) + l_r\left(F_{b,RL} + F_{b,RR}\right) \end{aligned} \tag{3}$$

where, t_f and t_r denote the width of the vehicle at the front and rear, respectively; $F_{b,*}$ denotes the damping force of $* = \{FL\ FR\ RL\ RR\}$, i.e. front-left, front-right, rear-left, and rear-right, respectively.

However, since the yaw moment is indirectly influenced by the changes in vertical force generated by the ECS, it is difficult to define this relationship in an equation. In this paper, the equation of the yaw moment is derived using lateral force changes according to left and right load transfer. The lateral force for the load can be defined as follows [22]:

$$F_y = \left(aF_z - bF_z^2\right)\alpha \tag{4}$$

where, a and b denote tuning parameters; α denotes the tire slip angle; F_y and F_z are the lateral and vertical forces, respectively.

From (4), the vertical force of each wheel can be defined as,

$$F_{z,i} = F_{z,i} + \Delta F_{z,i} + F_{b,i}, \quad i = FL,\ FR,\ RL,\ RR \tag{5}$$

where, $\Delta F_{z,i}$ denotes the vertical force change due to maneuvering, i.e. an acceleration or deceleration; $F_{z,i}$ denotes the static vertical force.

Substituting (5) into (4), then the front and rear lateral forces can be written as follows:

$$\begin{aligned} F_{y,F} &= F_{y,FL} + F_{y,FR} \\ &= \left(e_1F_{b,FL} + e_2F_{b,FL}^2 + e_3F_{b,FR} + e_2F_{b,FR}^2 + e_4\right)\alpha_f \\ F_{y,R} &= F_{y,RL} + F_{y,RR} \\ &= \left(g_1F_{b,RL} + g_2F_{b,RL}^2 + g_3F_{b,RR} + g_2F_{b,RR}^2 + g_4\right)\alpha_r \end{aligned} \tag{6}$$

where,

$$\begin{aligned} e_1 &= \left(a - 2b\left(F_{z,F} + \Delta F_{z,FL}\right)\right), \quad e_2 = -b, \\ e_3 &= a\left(2F_{z,F} + \Delta F_{z,FL} + \Delta F_{z,FR}\right) \\ e_4 &= a\left(2F_{z,F} + \Delta F_{z,FL} + \Delta F_{z,FR}\right) - b\left(F_{z,F} + \Delta F_{z,FL}\right)^2 \\ &\quad - b\left(F_{z,F} + \Delta F_{z,FR}\right)^2 \\ g_1 &= \left(a - 2b\left(F_{z,R} + \Delta F_{z,RL}\right)\right), \quad g_2 = -b, \\ g_3 &= a\left(2F_{z,R} + \Delta F_{z,RL} + \Delta F_{z,RR}\right) \\ g_4 &= a\left(2F_{z,R} + \Delta F_{z,RL} + \Delta F_{z,RR}\right) - b\left(F_{z,R} + \Delta F_{z,RL}\right)^2 \\ &\quad - b\left(F_{z,R} + \Delta F_{z,RR}\right)^2 \end{aligned}$$

where, e_i and g_i $(i = 1, \ldots, 4)$ are variables derived during the calculation process.

From (6), the relationship between the yaw moment and the damping forces can be derived as follows:

$$\begin{aligned} M_z &= l_fF_{y,F} - l_rF_{y,R} \\ &= \left(e_1F_{b,FL} + e_2F_{b,FL}^2 + e_3F_{b,FR} + e_2F_{b,FR}^2 + e_4\right)\alpha_f \\ &\quad - \left(g_1F_{b,RL} + g_2F_{b,RL}^2 + g_3F_{b,RR} + g_2F_{b,RR}^2 + g_4\right)\alpha_r \end{aligned} \tag{7}$$

From (7), it can be seen that there are squares for the ECS damping forces. This nonlinear equation is non-convex, which has disadvantages when it comes to optimization. To solve this problem, the Taylor series approach is applied to linearize (6) as follows:

$$\begin{aligned} &F_{y,F}\left(x_1, x_2\right) \\ &\approx F_{y,F}\left(a_1, a_2\right) + \left(x_1 - a_1\right)\frac{\partial F_{y,F}\left(x_1, x_2\right)}{\partial x_1}\bigg|_{\substack{x_1 = a_1, \\ x_2 = a_2}} \\ &\quad + \left(x_2 - a_2\right)\frac{\partial F_{y,F}\left(x_1, x_2\right)}{\partial x_2}\bigg|_{\substack{x_1 = a_1, \\ x_2 = a_2}} \end{aligned} \tag{8}$$

where, $x_1 = F_{b,FL}(k)$, $x_2 = F_{b,FR}(k)$, $a_1 = F_{b,FL}(k-1)$, and $a_2 = F_{b,FR}(k-1)$.

(8) is the linearization of the front wheel lateral force, the same approach is applied for the rear wheel lateral force. In this way, the linear equation for yaw moment is derived as,

$$M_z \approx l_f\left(\eta_{f1}F_{b,FL} + \eta_{f2}F_{b,FR}\right) - l_r\left(\eta_{r1}F_{b,RL} + \eta_{r2}F_{b,RR}\right) \tag{9}$$

where, $\eta_*, ^* = \{f1\ f2\ r1\ r2\}$ is derived from (7) and (8). Using (3) and (9), the cost function for the optimization can be defined as follows:

$$\min_u J = u^T R u + s^T Q s$$
$$where,$$
$$u = \begin{bmatrix} F_{b,FL} & F_{b,FR} & F_{b,RL} & F_{b,RR} \end{bmatrix},$$
$$s = \begin{bmatrix} M_x - \left[\frac{t_f}{2}\left(F_{b,FL} - F_{b,FR}\right) + \frac{t_r}{2}\left(F_{b,RL} - F_{b,RR}\right)\right] \\ M_y - \left[-l_f\left(F_{b,FL} + F_{b,FR}\right) + l_r\left(F_{b,RL} + F_{b,RR}\right)\right] \\ M_z - \begin{bmatrix} l_f\left(\eta_{f1}F_{b,FL} + \eta_{f2}F_{b,FR}\right) \\ -l_r\left(\eta_{r1}F_{b,RL} + \eta_{r2}F_{b,RR}\right) \end{bmatrix} \end{bmatrix}$$
$$\mathbf{Q} = diag\begin{bmatrix} q_1 & q_2 & q_3 \end{bmatrix}, \quad \mathbf{R} = diag\begin{bmatrix} r_1 & r_2 & r_3 & r_4 \end{bmatrix} \quad (10)$$

where, $\boldsymbol{J}$ denotes the cost to minimize; $\boldsymbol{Q}$ denotes the weighting matrix to control the roll angle, pitch angle, and yaw rate behaviors with values in the range 0 to 100. $\boldsymbol{R}$ denotes the weighting matrix for ECS control at each wheel. In this paper, we set r_1 to r_4 to be identical because each wheel has the same actuator.

To obtain the optimal damping force, $\boldsymbol{J}$ is partially differentiated as follows:

$$\frac{\partial J}{\partial F_{b,FL}} = 2r_1F_{b,FL} - q_1t_f\left[M_x - \begin{Bmatrix} \frac{t_f}{2}\left(F_{b,FL} - F_{b,FR}\right) \\ +\frac{t_r}{2}\left(F_{b,RL} - F_{b,RR}\right) \end{Bmatrix}\right] + 2q_2l_f\left[M_y - \begin{Bmatrix} -l_f\left(F_{b,FL} + F_{b,FR}\right) \\ +l_r\left(F_{b,RL} + F_{b,RR}\right) \end{Bmatrix}\right] - 2q_3l_f\eta_{f1}\left[M_z - \begin{Bmatrix} l_f\left(\eta_{f1}F_{b,FL} + \eta_{f2}F_{b,FR}\right) \\ -l_r\left(\eta_{r1}F_{b,RL} + \eta_{r2}F_{b,RR}\right) \end{Bmatrix}\right] = 0$$

$$\frac{\partial J}{\partial F_{b,FR}} = 2r_2F_{b,FR} + q_1t_f\left[M_x - \begin{Bmatrix} \frac{t_f}{2}\left(F_{b,FL} - F_{b,FR}\right) \\ +\frac{t_r}{2}\left(F_{b,RL} - F_{b,RR}\right) \end{Bmatrix}\right] + 2q_2l_f\left[M_y - \begin{Bmatrix} -l_f\left(F_{b,FL} + F_{b,FR}\right) \\ +l_r\left(F_{b,RL} + F_{b,RR}\right) \end{Bmatrix}\right] - 2q_3l_f\eta_{f2}\left[M_z - \begin{Bmatrix} l_f\left(\eta_{f1}F_{b,FL} + \eta_{f2}F_{b,FR}\right) \\ -l_r\left(\eta_{r1}F_{b,RL} + \eta_{r2}F_{b,RR}\right) \end{Bmatrix}\right] = 0$$

$$\frac{\partial J}{\partial F_{b,RL}} = 2r_3F_{b,RL} - q_1t_r\left[M_x - \begin{Bmatrix} \frac{t_f}{2}\left(F_{b,FL} - F_{b,FR}\right) \\ +\frac{t_r}{2}\left(F_{b,RL} - F_{b,RR}\right) \end{Bmatrix}\right] - 2q_2l_r\left[M_y - \begin{Bmatrix} -l_f\left(F_{b,FL} + F_{b,FR}\right) \\ +l_r\left(F_{b,RL} + F_{b,RR}\right) \end{Bmatrix}\right] + 2q_3l_r\eta_{r1}\left[M_z - \begin{Bmatrix} l_f\left(\eta_{f1}F_{b,FL} + \eta_{f2}F_{b,FR}\right) \\ -l_r\left(\eta_{r1}F_{b,RL} + \eta_{r2}F_{b,RR}\right) \end{Bmatrix}\right] = 0$$

$$\frac{\partial J}{\partial F_{b,RR}} = 2r_4F_{b,RR} + q_1t_r\left[M_x - \begin{Bmatrix} \frac{t_f}{2}\left(F_{b,FL} - F_{b,FR}\right) \\ +\frac{t_r}{2}\left(F_{b,RL} - F_{b,RR}\right) \end{Bmatrix}\right] - 2q_2l_r\left[M_y - \begin{Bmatrix} -l_f\left(F_{b,FL} + F_{b,FR}\right) \\ +l_r\left(F_{b,RL} + F_{b,RR}\right) \end{Bmatrix}\right] + 2q_3l_r\eta_{r2}\left[M_z - \begin{Bmatrix} l_f\left(\eta_{f1}F_{b,FL} + \eta_{f2}F_{b,FR}\right) \\ -l_r\left(\eta_{r1}F_{b,RL} + \eta_{r2}F_{b,RR}\right) \end{Bmatrix}\right] = 0 \quad (11)$$

where, $F_{b,i}$ denotes the optimal damping force of each actuator ($i = FL, FR, RL, RR$).

Using (11), the optimal damping force for the ECS can be computed. This approach is used equally in the 1st and 2nd optimization module.

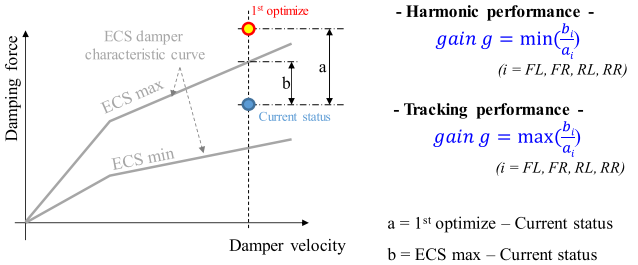

FIGURE 5. Conceptual diagram for "gain g".

2) CONTROL VALUE COMPENSATION MODULE

In the previous section, the optimal damping force was calculated with an unconstrained optimization approach. However, the ECS system is a semi-active system with very limited controllable damping force. Therefore, the optimum damping forces calculated are likely to exceed the performance limits of the ESC system. It can be seen from Fig. 4 that if this optimum damping force is used as the final control value, while the tracking performance might be satisfactory, good harmonic performance cannot be guaranteed. In order to consider the performance limit of the ECS system and facilitate adjustments between the tracking and harmonic performance, the "gain g" is computed in the control value compensation module. The control moments (yaw, roll, pitch) determined by the IVC module are scaled to fit the limitations of the system through "gain g". The damping forces optimized with these scaled control moments do not exceed the limits of the system. The "gain g" can be computed as shown in Fig. 5 using the damping force from the 1st optimization, the current damping force, and the min/max damping force values of the ECS system. Since the ECS system is independently mounted on each wheel, the calculated "gain g" has a total of four values. If the maximum of these values is used as the "gain

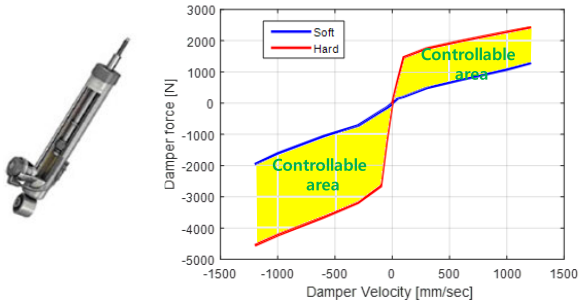

FIGURE 6. Damper characteristics of the ESC system.

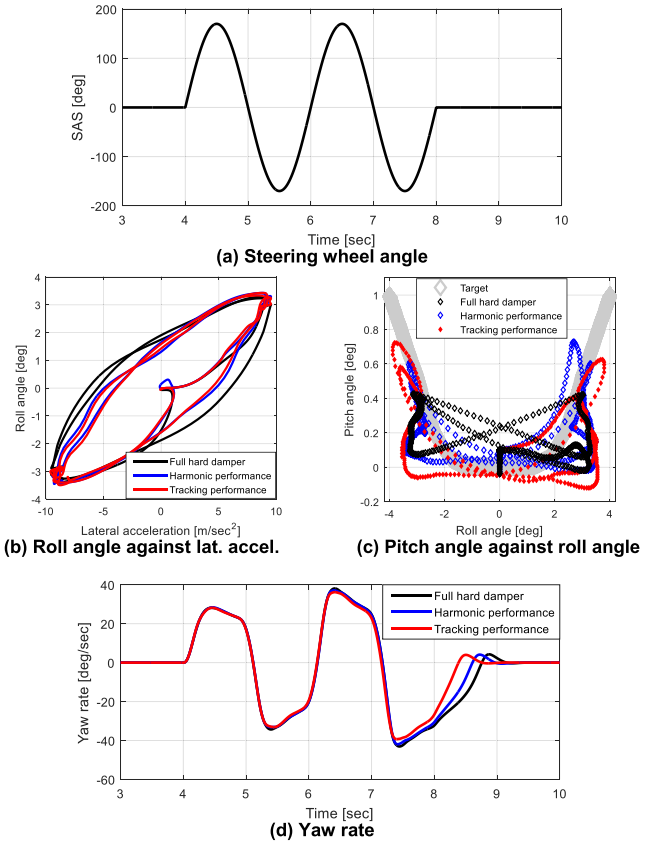

FIGURE 7. Simulation results for the double sine maneuver @ 80 km/h.

g", the tracking performance can be achieved. Conversely, when the minimum value is used, the harmonic performance is achieved. This can be seen in Fig. 4.

III. EVALUATION

To evaluate the proposed control algorithm, simulated and experimental tests were conducted. In the case of the simulations, they were performed to show the difference between the tracking and harmonic performance. The experimental tests for the harmonic performance were conducted to investigate weight tuning between target moments (M_x, M_y, M_z). Fig. 6 shows the damper characteristics of the ESC system used in the simulations and vehicle tests.

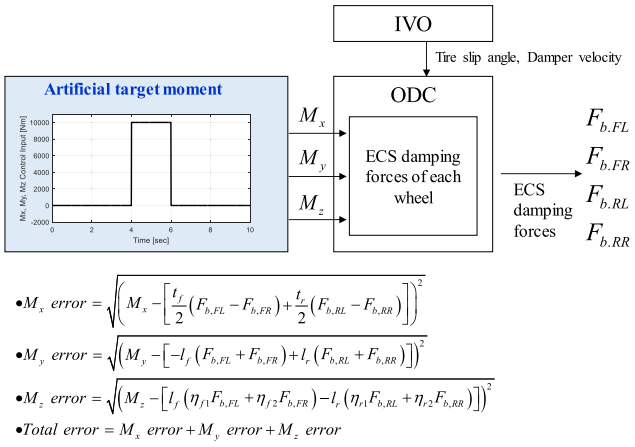

FIGURE 8. Evaluation method (tracking/harmonic performance).

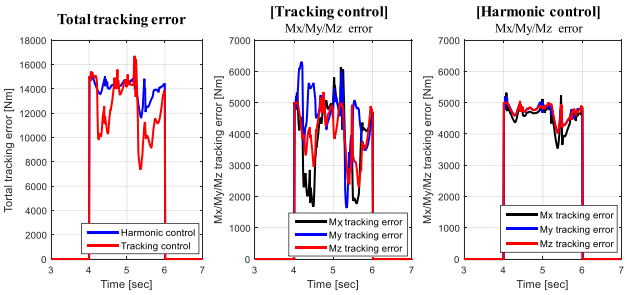

FIGURE 9. Evaluation results (tracking/harmonic performance).

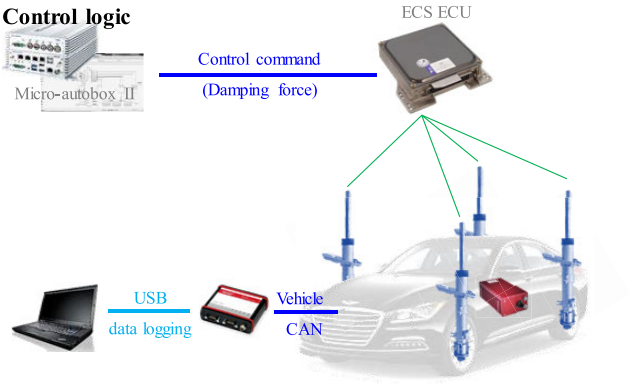

FIGURE 10. Test vehicle configuration.

A. SIMULATION EVALUATION

The computer simulations using CARSIM and Matlab/Simulink were performed to evaluate the tracking and harmonic performance of the proposed algorithm. A double sine maneuver on an asphalt road ($\mu = 0.85$) was simulated. The initial speed was set to 90 km/h, constant throttle input was applied during the simulation. The weights for the control moments were all equally assigned to 100. The time history of the steering angle is shown in Fig. 7-(a) while Fig. 7-(b)∼(d) shows the roll angle against lateral acceleration, the pitch angle against roll angle, and the yaw rate,

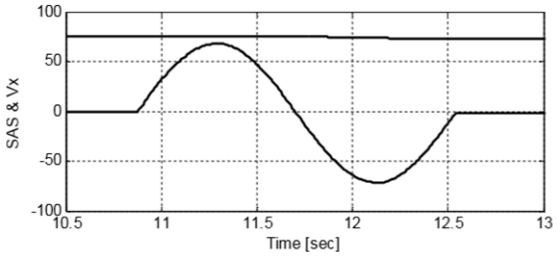

FIGURE 11. Test scenario (70 degree single lane change @ 80km/h).

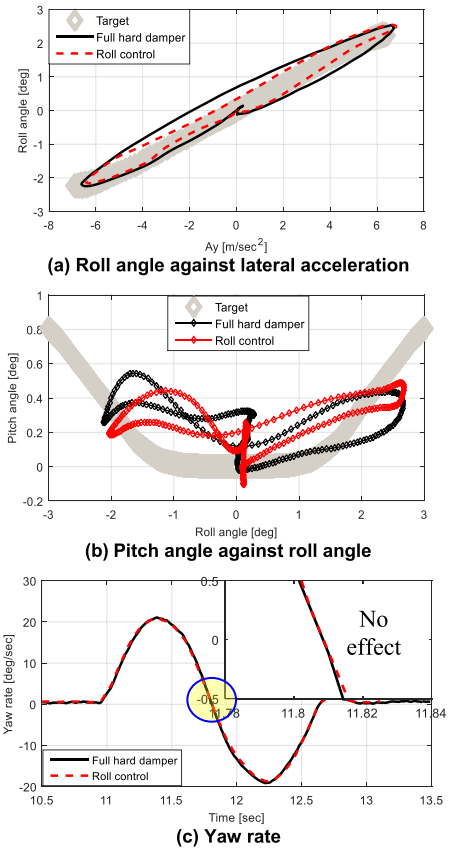

FIGURE 12. Case 1 results (no control vs roll control).

respectively. The solid black line, the blue solid line, and the red solid line represent the results from using the full hard damper setting, the harmonic control prioritized setting (minimum "gain g"), and the tracking control prioritized setting (maximum "gain g", respectively. As shown in Fig. 7-(b), the hysteresis width for both the harmonic control and the tracking control modes is smaller than that for the full hard damper setting. In addition, we can see in Fig. 7-(c) and (d) that by using the proposed control method, the pitch angle follows the target pitch angle and the yaw rate is more stable.

Unfortunately, these results cannot show the differences between the tracking and harmonic performance, since the target moments (M_x, M_y, M_z) have different values. To show the difference, the same target moments were artificially

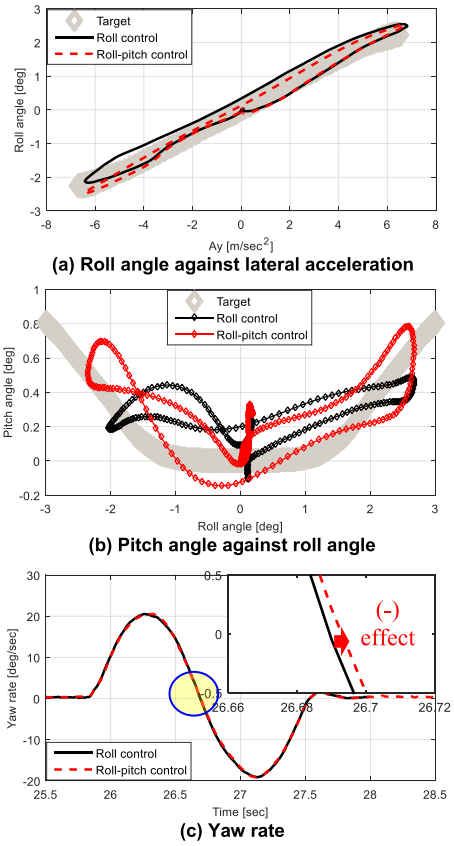

FIGURE 13. Case 2 results (roll control vs roll-pitch control).

applied to the same simulation scenario as above. The performances of each mode were evaluated by comparing the tracking errors for each target moment and the sum of these errors. Fig. 8 and 9 show the evaluation methods and results, respectively. Looking at Fig. 9, it can be seen that the tracking performance control mode has a smaller overall tracking error than the harmonic performance control mode, while the difference in tracking error to each target moment being large.

B. EXPERIMENTAL EVALUATION

To investigate the weight tuning performance between target moments using the proposed control algorithm, experimental tests were conducted. The proposed algorithm was implemented on the dSPACE autobox, an RT3002 unit was installed to measure the roll and pitch angles. The tests were conducted using a steering robot to ensure identical driving conditions. Fig. 10 shows the configuration of the test vehicle. The test scenario was a single lane change (SLC) with a lateral acceleration of 0.6g. The roll, pitch and yaw behaviors were analyzed as follows:

- Roll angle: roll response to the lateral acceleration
- Pitch angle: pitch response to the roll angle
- Yaw rate: yaw response to the steering angle

In order to analyze the harmonic performance, the minimum "gain g", was used. Since roll control is the main

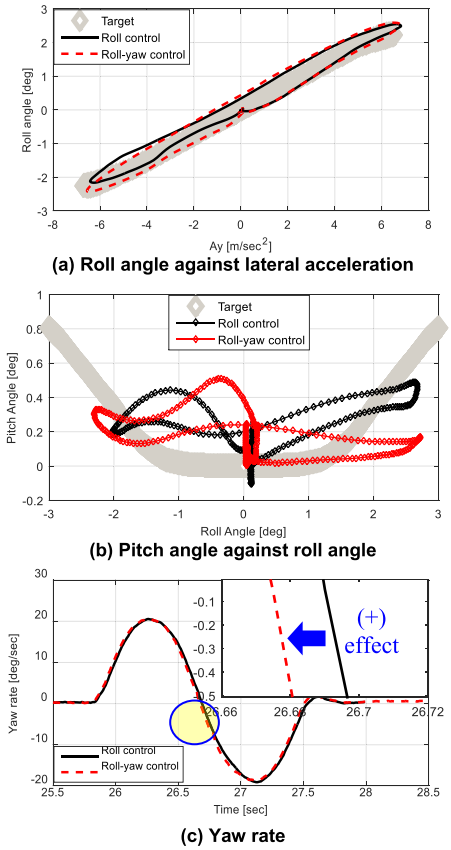

FIGURE 14. Case 3 results (roll control vs roll-yaw rate control).

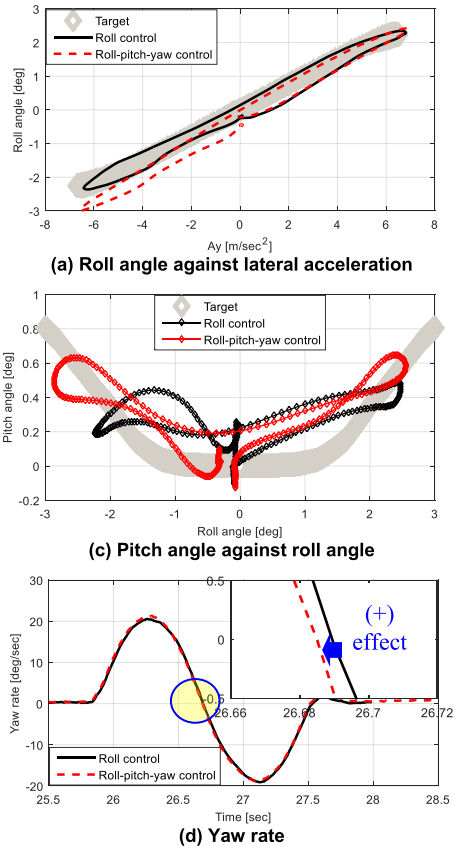

FIGURE 15. Case 4 results (roll control vs roll-pitch-yaw rate control).

TABLE 1. Performance comparison cases.

Case 1	No control(Full hard damper) vs. Roll control None vs. (q_1:q_2:q_3 = **100**:0:0)
Case 2	Roll control vs. Roll-pitch control (q_1:q_2:q_3 = **100**:0:0) vs. (q_1:q_2:q_3 = **100:100**:0)
Case 3	Roll control vs. Roll-yaw control (q_1:q_2:q_3 = **100**:0:0) vs. (q_1:q_2:q_3 = **100**:0:**100**)
Case 4	Roll control vs. Roll-pitch-yaw control (q_1:q_2:q_3 = **100**:0:0) vs. (q_1:q_2:q_3 = **100**:**100**:**100**)

function of the ECS, the performance is compared based on this. Table 1 shows the performance comparison cases. In Case 1, roll control and no control are compared. In the case of the no control, all dampers are set hard to stabilize the roll behavior. Case 2 and Case 3 compare the roll-pitch control and roll-yaw control, respectively, with roll control. In the last test, Case 4, the roll-pitch-yaw control is compared with roll control.

Fig. 11 shows the steering angle and vehicle speed during the tests using the steering robot. 70 degree SLC steering input at 0.6 kHz was performed at 80 km/h.

Fig. 12 shows the vehicle test results for Case 1. As shown in Fig. 12-(a), the hysteresis width using roll control is smaller than that under full hard dampers. Roll control allows the relationship between the roll angle and the lateral acceleration to be more linear. Fig. 12-(b) describes the pitch angle against roll angle. The pitch angle shows a positive value because of the deceleration caused by the steering angle during lane change. Also, in Case 1, only the roll angle is controlled, so the pitch angle behavior is not improved. Fig. 12-(c) shows the yaw rate. In a similar way to the pitch behavior, the yaw rate response is not improved.

Fig. 13 shows the performance comparison results for Case 2 where the roll control is compared to roll-pitch control. Fig. 13-(b) shows the pitch angle against roll angle. When using roll-pitch control, the pitch angle follows the target value better. However, it can be seen from Fig. 13-(a) that the peak roll angle value is increased compared to using roll control. This is because the damping forces that were used only for roll control are now distributed to control the roll and pitch. The yaw behavior is the same because yaw rate control is not performed in Case 2.

Fig. 14 shows the results for Case 3, it shows that the yaw response is improved and the pitch behavior is not controlled so shows no improvement. As can be seen in Fig. 14-(a), the roll angle peak value is increased in a similar way to in Case 2.

Fig. 15 shows the results for the roll-pitch-yaw rate control. The results show that the yaw response is improved

and the pitch angle also tracks the target value well. However, as the damping forces are distributed to control roll angle, pitch angle, and yaw rate control, the roll angle is the large. Also, the performance of the pitch angle and yaw rate are slightly decreased compared to Case 2 and Case3, respectively.

IV. CONCLUSION

An integrated vehicle motion control system was developed to simultaneously control the roll, pitch, and yaw behavior of a vehicle using an electronic control suspension (ECS) system. The proposed algorithm consists of four modules: (i) an integrated vehicle observer (IVO), (ii) an integrated target generator (ITG), (iii) an integrated vehicle controller (IVC), and (iv) an optimal distribution controller (ODC). The ITG computes the target roll angle, pitch angle and yaw rate of the vehicle. The IVC computes the roll, pitch, and yaw moments to track the target behavior. The ODC computes the ECS damping force at each wheel to follow the moments provided by the IVC. The ODC has two non-constrained optimization modules and a control value compensation module that consider the ECS system limitations. This module also has the advantage of being able to easily obtain the desired results in experimental vehicle tests because the weights for roll, pitch, and yaw control can be adjusted along with being able to tune the balance between tracking performance and harmonic performance. To evaluate the proposed control algorithm, simulated and experimental tests were conducted. The differences between tracking performance control and the harmonic performance control modes were confirmed through simulations. As a result of the experimental tests, it was also confirmed that the roll angle, pitch angle, and yaw rate of a vehicle can be controlled as intended according to the setting of the weighting factors.

The contribution of this paper is the development of a control logic that can control each combination of roll-pitch-yaw behavior using ECS. One of the critical issues when developing the control logic to improve ride & handling (R&H) performance of vehicles is that it is not possible to define ''best'' R&H performance. The best R&H performance varies depending on the driver because it is a very subjective characteristic. The proposed algorithm is able to provide various vehicle behaviors through simple parameter tuning. Hence, in our future work we will try to achieve the best possible R&H performance by optimally tuning the weighting factors and the ''gain g''.

REFERENCES

[1] J. Zhao, P. K. Wong, X. Ma, and Z. Xie, ''Design and analysis of an integrated sliding mode control–two-point wheelbase preview strategy for a semi-active air suspension with stepper motor-driven gas-filled adjustable shock absorber,'' *Proc. Inst. Mech. Eng., I, J. Syst. Control Eng.*, vol. 232, no. 9, pp. 1194–1211, 2018.

[2] X. Ma, P. K. Wong, and J. Zhao, ''Adaptive regulating of automotive mono-tube hydraulic adjustable dampers using gray neural network–based compensation system,'' *Proc. Inst. Mech. Eng., D, J. Automobile Eng.*, vol. 233, no. 10, pp. 2532–2545, 2019.

[3] H. E. Tseng and D. Hrovat, ''State of the art survey: Active and semi-active suspension control,'' *Vehicle Syst. Dyn.*, vol. 53, no. 7, pp. 1034–1062, May 2015.

[4] D. Fischer and R. Isermann, ''Mechatronic semi-active and active vehicle suspensions,'' *Control Eng. Pract.*, vol. 12, no. 11, pp. 1353–1367, Nov. 2004.

[5] M. Sunwoo, K. C. Cheok, and N. J. Huang, ''Model reference adaptive control for vehicle active suspension systems,'' *IEEE Trans. Ind. Electron.*, vol. 38, no. 3, pp. 217–222, Jun. 1991.

[6] T. Merker, G. Girres, and O. Thriemer, ''Active body control (ABC) the DaimlerChrysler active suspension and damping system,'' SAE Tech. Paper 2002-21-0054, Oct. 2002.

[7] A. B. Sharkawy, ''Fuzzy and adaptive fuzzy control for the automobiles' active suspension system,'' *Vehicle Syst. Dyn.*, vol. 43, no. 11, pp. 795–806, Nov. 2005.

[8] S. M. Savaresi, C. Poussot-Vassal, and C. Spelta, *Semi-Active Suspension Control Design for Vehicles*. Amsterdam, The Netherlands: Elsevier, 2011.

[9] X. Ma, P. K. Wong, and J. Zhao, ''Practical multi-objective control for automotive semi-active suspension system with nonlinear hydraulic adjustable damper,'' *Mech. Syst. Signal Process.*, vol. 117, pp. 667–688, Feb. 2019.

[10] W. Huang, J. Zhao, G. Yu, and P. K. Wong, ''Intelligent vibration control for semi-active suspension systems without prior knowledge of dynamical nonlinear damper behaviors based on improved extreme learning machine,'' *IEEE/ASME Trans. Mechatronics*, early access, Oct. 16, 2020, doi: 10.1109/TMECH.2020.3031840.

[11] X. Jin, J. Wang, S. Sun, S. Li, J. Yang, and Z. Yan, ''Design of constrained robust controller for active suspension of in-wheel-drive electric vehicles,'' *Mathematics*, vol. 9, no. 3, p. 249, Jan. 2021.

[12] J. J. Rath, M. Defoort, C. Sentouh, H. R. Karimi, and K. C. Veluvolu, ''Output-constrained robust sliding mode based nonlinear active suspension control,'' *IEEE Trans. Ind. Electron.*, vol. 67, no. 12, pp. 10652–10662, Dec. 2020.

[13] Z. Tianjun and Z. Hongyan, ''Roll control of SUV using semi-active suspension based on SIA control,'' in *Proc. Int. Conf. Inf. Technol. Comput. Sci.*, Kiev, Ukraine, Jul. 2009, pp. 589–592, doi: 10.1109/ITCS.2009.128.

[14] K. Lee, Y. Kim, and J. Jang, ''A study of integrated chassis control algorithm with brake control and suspension control systems for vehicle stability and handling performance,'' in *Proc. ICCAS-SICE*, Fukuoka, Japan, Aug. 2009, pp. 4053–4057.

[15] J. Zhao, P. K. Wong, X. Ma, and Z. Xie, ''Chassis integrated control for active suspension, active front steering and direct yaw moment systems using hierarchical strategy,'' *Vehicle Syst. Dyn.*, vol. 55, no. 1, pp. 72–103, Oct. 2016.

[16] X. Jin, J. Yang, Y. Li, B. Zhu, J. Wang, and G. Yin, ''Online estimation of inertial parameter for lightweight electric vehicle using dual unscented Kalman filter approach,'' *IET Intell. Transp. Syst.*, vol. 14, no. 5, pp. 412–422, May 2020.

[17] W. Cho, J. Yoon, S. Yim, B. Koo, and K. Yi, ''Estimation of tire forces for application to vehicle stability control,'' *IEEE Trans. Veh. Technol.*, vol. 59, no. 2, pp. 638–649, Feb. 2010.

[18] A. Rezaeian, R. Zarringhalam, S. Fallah, W. Melek, A. Khajepour, S.-K. Chen, N. Moshchuck, and B. Litkouhi, ''Novel tire force estimation strategy for real-time implementation on vehicle applications,'' *IEEE Trans. Veh. Technol.*, vol. 64, no. 6, pp. 2231–2241, Jun. 2015.

[19] H. Pan, W. Sun, H. Gao, T. Hayat, and F. Alsaadi, ''Nonlinear tracking control based on extended state observer for vehicle active suspensions with performance constraints,'' *Mechatronics*, vol. 30, pp. 363–370, Sep. 2015.

[20] B. Li, H. Du, W. Li, and Y. Zhang, ''Side-slip angle estimation based lateral dynamics control for omni-directional vehicles with optimal steering angle and traction/brake torque distribution,'' *Mechatronics*, vol. 30, pp. 348–362, Sep. 2015.

[21] T. Kodaira, Y. Yamamoto, H. Sakai, Y. Muragishi, K. Fukui, and E. Ono, ''Improvement of vehicle dynamics based on human sensitivity (Second Report)-a study of cornering feel,'' SAE Tech. Paper 2007-01-0447, Apr. 2007.

[22] W. Cho, J. Choi, C. Kim, S. Choi, and K. Yi, ''Unified chassis control for the improvement of agility, maneuverability, and lateral stability,'' *IEEE Trans. Veh. Technol.*, vol. 61, no. 3, pp. 1008–1020, Mar. 2012.

[23] T. D. Gillespie, *Fundamentals of Vehicle Dynamics*. Warrendale, PA, USA: SAE International, 1992.

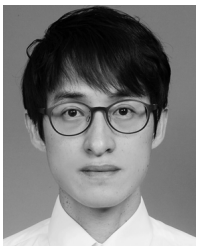

WANKI CHO received the B.S. degree in mechanical engineering from Hanyang University, Seoul, South Korea, in 2004, and the M.S. and Ph.D. degrees in mechanical and aerospace engineering from Seoul National University, Seoul, in 2006 and 2011, respectively. From 2011 to 2019, he was a Senior Research Engineer with the Automotive Research and Development Division, Hyundai Motor Group, South Korea. He is currently an Assistant Professor with the School of Mechanical Engineering, Korea University of Technology and Education. His research interests include integrated chassis control systems, and intelligent vehicle control.

JONGSANG SUH received the B.S. and Ph.D. degrees in mechanical engineering from Seoul National University, South Korea, in 2012 and 2016, respectively. From 2017 to 2019, he is a Postdoctoral Researcher in mechanical engineering with the University of California, Berkeley, USA. He is currently a Senior Control Engineer with Phantom AI, USA. His research interests include self-driving vehicle control with stochastic model predictive control theory and vision-based SLAM.

SEUNG-HAN YOU received the B.S., M.S., and Ph.D. degrees in mechanical and aerospace engineering from Seoul National University, Seoul, South Korea, in 1999, 2001, and 2006, respectively. From 2006 to 2015, he was a Senior Research Engineer with the Automotive Research and Development Division, Hyundai Motor Group, South Korea. Since 2015, he has been with the School of Mechanical Engineering, Korea University of Technology and Education, where he is currently an Associate Professor. His current research interests include control systems, state estimations, parameter estimations, and their applications in future vehicles.